Journal of Geophysical Research Oceans
September 2009, Volume 114 (C09007) : Pages 1-17
http://dx.doi.org/10.1029/2008JC005237

An edited version of this paper was published by AGU.

Global hydrographic variability patterns during 2003–2008

K. von Schuckmann[1, *], F. Gaillard[1] and P.-Y. Le Traon[2]

[1] LPO, UMR 6523, UBO, Ifremer, IRD, CNRS, Plouzané, France
[2] LOS, Ifremer, Plouzané, France

*: Corresponding author : K. von Schuckmann, email address : Karina.Von.Schuckmann@ifremer.fr

Abstract:

Monthly gridded global temperature and salinity fields from the near-surface layer down to 2000 m depth based on Argo measurements are used to analyze large-scale variability patterns on annual to interannual time scales during the years 2003–2008. Previous estimates of global hydrographic fluctuations have been derived using different data sets, partly on the basis of scarce sampling. The substantial advantage of this study includes a detailed summary of global variability patterns based on a single and more uniform database. In the upper 400 m, regions of strong seasonal salinity changes differ from regions of strong seasonal temperature changes, and large amplitudes of seasonal salinity are observed in the upper tropical and subpolar global ocean. Strong interannual and decadal changes superimpose long-term changes at northern midlatitudes. In the subtropical and tropical basin, interannual fluctuations dominate the upper 500 m depth. At southern midlatitudes, hydrographic changes occur on interannual and decadal time scales, while long-term changes are predominantly observed in the salinity field. Global mean heat content and steric height changes are clearly associated with a positive trend during the 6 years of measurements. The global 6-year trend of steric height deduced from in situ measurements explains 40% of the satellite-derived quantities. The global freshwater content does not show a significant trend and is dominated by interannual variability.

1. Introduction

Monitoring the variability of ocean temperature and salinity properties on interannual to decadal time scales is essential to understand the climate system. Global observing arrays have been set up in order to provide the necessary datasets. Satellite observations give access to surface currents and the total volume but fail to describe the internal distribution of density. The relative contribution of heat and salt to these density changes are also out of reach of the remote sensing techniques. In situ measurements are thus the only possibility for describing this type of variability.

Global baroclinic variability reflects the motion of the main thermocline [*Wunsch*, 1997] and its geographical distribution shows a strong resemblance to mean dynamical structures [*Forget and Wunsch*, 2007]. The largest signal of global hydrographic variability is associated with the annual cycle. Strongest seasonal sea surface temperature (SST) changes occur at mid-latitudes and are larger in the northern hemisphere, reflecting the contrast between the two hemispheres in the distribution of land mass [*Fu and Cazenave*, 2001; *Antonov et al.*, 2004]. The geographical distribution of seasonal sea surface salinity (SSS) fluctuations strongly differs from the one observed in the temperature field [*Boyer and Levitus*, 2002].

Low-frequency ocean variability is often controlled by changes in modes of the atmospheric circulation [*Palmer et al.*, 2007]. The largest source of climate variability in the instrumental record is El Niño Southern Oscillation (ENSO) associated with large amounts of interannual hydrographic variability in the upper layer of the tropical basin [e.g. *Willis et al.*, 2004]. The Indian Ocean Dipole (IOD) leads to basin wide hydrographic fluctua-

tions at interannual time scales in the tropical Indian Ocean [e.g. *Saji et al.*, 1999]. In the tropical Atlantic, two primary modes of interannual climate variability occur, i.e. an equatorial and a meridional mode [*Servain et al.*, 1999]. Variability at interannual periods of ocean circulation in the North Atlantic is related to the North Atlantic Oscillation [NAO, *Eden and Willebrand*, 2001]. In the North Pacific, large interannual fluctuations are controlled by the Pacific Decadal Oscillation (PDO) [*Harrison and Carson*, 2007; *Carton et al.*, 2008]. At southern mid-latitudes the principal mode of atmospheric forcing is the Southern Annular Mode (SAM) and oceanic fluctuations in this region are triggered by this atmospheric forcing as well as by the ENSO mode [*Sallée et al.*, 2008; *Morrow et al.*, 2008].

Owing to a lack of direct salinity observations, previous analyses on signatures of ocean interannual variability have often concentrated on the temperature field, assuming that changes in the density field result mostly from temperature changes. However, the salinity effect cannot be neglected. In the tropical Pacific, large fluctuations of SSS are controlled by ENSO [*Delcroix et al.*, 2005] and reach down to 175m depth [*Kessler*, 1998]. In the Atlantic Ocean, large-scale SSS interannual variabilities are in part related to ENSO and NAO [*Mignot and Frankignoul*, 2003; *Reverdin et al.*, 2007]. Salinity variability is also important to understand observed satellite derived sea level variations, especially in regions where the haline steric component plays a dominant role [*Antonov et al.*, 2002; *Munk*, 2003].

Long-term fluctuations and trends characterize the signal of ocean variability as well. Much of this variability is known to be related to atmospheric and anthropogenic forcings and it is difficult to identify its signatures as the oceans do not warm uniformly across

the globe [*Barnett et al.*, 2005]. Large parts of ocean heat content change has occured during the past 50 years in the upper 700m of the world ocean and the Atlantic Ocean contributes most to this increase [*Levitus et al.*, 2005, LE05, hereinafter]. In addition, the long-term global warming trend is also largly caused by warming in the Southern Ocean that extends deep into the water column [*Willis et al.*, 2004; *Sallée et al.*, 2008]. In the tropical basin warming and cooling patterns are shallow and large amounts of heat in the tropics are redistributed within the ocean, but little heat is lost or gained in the global average [*Willis et al.*, 2004; *Good et al.*, 2007].

Large-scale coherent trends are also detected in the salinity field during the past 50 years. In the Pacific Ocean a freshening trend occurs in the tropical basin [*Antonov et al.*, 2002; *Delcroix et al.*, 2007]. In the Atlantic Ocean evidence of a deep freshening in the northern subpolar gyre is documented whereas in the subtropics and tropics an increase in salinity can be observed [*Curry et al.*, 2003; *Boyer et al.*, 2005]. In the Southern Ocean a large-scale deep freshening is reported, predominantly in the Pacific and Indian Ocean [*Wong et al.*, 1999; *Antonov et al.*, 2002; *Böning et al.*, 2008]. Moreover, a freshening signal can be observed in both the Weddel and Ross Seas [*Boyer et al.*, 2005]. The Indian Ocean is dominated by an increase in salinity in the upper layer and a freshening in the subsurface layer at the equator and at 40°S [*Boyer et al.*, 2005].

Strong increase of sea level associated with steric expansion has been observed in the Pacific and Atlantic [*Antonov et al.*, 2005; *Häkkinen and Rhines*, 2004; *Douglass et al.*, 2006; *Cummins and Freeland*, 2007] and in the Southern Ocean [*Lombard et al.*, 2005; *Roemmich et al.*, 2007; *Willis et al.*, 2007; *Morrow et al.*, 2008]. *Antonov et al.* [2002] indicate that global freshwater changes also cause a contribution to sea level rise. Fur-

thermore, *Cazenave et al.* [2009] argue that freshwater inflow from the continents (mass changes) strongly contribute to the increase of total sea level for the last four years. However, these results strengthen on the one hand the discussion of the major causes of the global sea level rise derived from tide gauge measurements [*Church and White*, 2006] as for example discussed by *Munk* [2003]. On the other hand, it also shows the need to further compare and validate the global observing systems [*Willis et al.*, 2008].

The previous findings and remaining puzzles show that analyses of global observing systems are needed to fully describe key regions of large scale ocean variability. With the implementation of the Argo array [*Roemmich and Gould*, 2003] a major step was made to set up a truly global observing system for temperature and salinity of the upper 2000m depth. This study provides a detailed summary of annual to long-term variability patterns of the global ocean based on a uniform Argo data base. The paper is organized as follows. The gridded field is introduced in section 2. In section 3 we carry out a detailed description of long-term and seasonal hydrographic changes in the water column down to 2000m. Section 4 includes a description of global interannual fluctuations. Conclusions are given in the last section.

2. ARIVO: A gridded field of hydrographic measurements

2.1. Measurements and analysis method

The basic materials for this study are the monthly gridded fields of temperature and salinity properties of the upper 2000m over the period 2003-2008. These fields were obtained by optimal analysis of the large in-situ data set provided by the Argo array of profiling floats (www.argo.net). Complementary measurements from drifting buoys, CTDs and moorings are also used. Two important data sets have been excluded from the

analysis because of proven or suspected biases. They are first, the XBTs and XCTDs for which uncertainties in the accuracy of the fall rate remain, and second, a small subset of Argo float profiles of type SOLO (Sounding Oceanographic Lagrangian Observer) that suffer a labelling error in the pressure [*Willis et al.*, 2007]. The data set was downloaded from the Coriolis data center (one of Argo Global Data Acquisition Center, GDAC) at three dates: the period 2003-2006 was extracted in August 2007, the year 2007 in January 2008 and the year 2008 in February 2009. In total, the Argo measurements account for at least 90% in 2003 and increase to more than 95% since 2006.

The In-Situ Analysis System (ISAS) designed to reconstruct temperature and salinity fields on depth levels [*Gaillard and Charraudeau*, 2008] is based on the gridding method derived from estimation theory [*Liebelt*, 1967; *Bretherton et al.*, 1976]. This method is described in more details in *Gaillard et al.* [2009], but is shortly summarized below. The interpolated field, represented by the state vector x, is constructed as the departure from the reference field values at each grid point x^f. The anomaly is estimated by applying a gain matrix $\mathbf{K}^{OI}$ on the unpredicted part of the data $y^o - y^f$:

$$x^a = x^f + \mathbf{K}^{OI}\left(y^o - y^f\right) \quad (1)$$

$$P^a = P^f - \mathbf{K}^{OI} C_{oa}^T \quad , \quad (2)$$

$$\mathbf{K}^{OI} = C_{oa}(C_{oo} + R)^{-1} \quad , \quad (3)$$

where P^f is the a priori covariance of the field at grid points, C_{oa} the covariance matrix between analyzed and data points, C_{oo} the covariance matrix from data point to data point and R the observation noise covariance matrix.

The Coriolis data center produces in real time gridded fields of weekly temperature and salinity with a former version of ISAS (V3.6). We could have used this product

(hereafter named CORA) but we preferred to compute a new product that we name ARIVO (Analyse, Reconstruction et Indicateurs de la Variabilité Océanique), using the latter version of ISAS (V4) that offers a number of improvements. We summarize here the main characteristics of ARIVO, and point out the differences with CORA. Some of them are ascribable to the software version, others to different choices of the parameters.

ARIVO analysis is based on the same data set as CORA: uncorrected data assumed of good quality by the automatic quality control (QC-flags = 1 or 2) are used [*Argo Data Management*, 2005]. The data processing has been improved in ISAS-V4 that now performs additional controls against climatology and spike detection. For example, this screening has detected 600 profiles with anomalies in 2007. These erroneous points have been removed before analysis.

The configuration is defined by the grid and the set of a priori information such as the climatology, a priori variances and covariances which are necessary to compute the covariance matrices. The analyzed field is defined on a horizontal 1/2° Mercator isotropic grid and is limited from 77°S to 77°N. There are 152 vertical levels defined between the surface and 2000m depth (59 levels in CORA). The vertical spacing is 5m from the surface down to 100m depth, 10m from 100m to 800m and 20m from 800m down to 2000m depth. The reference field is the monthly World Ocean Atlas 2005 [WOA05, *Locarnini et al.*, 2006; *Antonov et al.*, 2006], whereas WOA98 is used in CORA.

Statistical information on the field and data noise are introduced through the covariance matrices that appear in Eq. 3. In CORA the variance was computed on the 2000-2004 data base and, given the reduced size of the data set, had to be averaged over large areas. In ARIVO the total variance is computed at each grid point as the variance - within a

5° square - of the anomaly of the 2002-2006 data set relative to the monthly WOA05 field. As for CORA, the covariance used in ARIVO results from the sum of two gaussian functions. The largest scale is set to 300 km, and the second scale is proportional to the Rossby Radius (bounded by the large scale). In CORA this scale was uniform over large areas, in ARIVO it is defined at each grid point. The analysis is performed once a month. In summary, we expect to have obtained gridded fields based on a cleaner data set, with improved resolution of the boundaries and fronts, a better estimate of the signal amplitude and a time sampling more adapted to the study of interannual variability.

2.2. Errors of the analyzed field

The information gain is measured by the statistical variance of the estimation (σ^2_{ei}), given by the diagonal P^a (Eq. 2), expressed as the percentage of a priori variance (σ^2_{xi}). The lower the percentage the higher the information extracted from the measurements. Where it equals 100% no information has been gained and the field remains identical to the reference field WOA05. The percentage of a priori variance (PAPV) varies inversely to the data density and our maps of mean PAPV (Fig. 2) can be compared to the maps of 'Observed area coverage' produced by *Lyman and Johnson* [2008] over a similar period. Our level of 90% error corresponds to their 0.6 area coverage level and represents the limit of acceptable estimate.

The zonal average of PAPV over the global ocean delivers a overview on the latitude and depth limits of the estimate (Fig. 1a and b). Temperature and salinity cannot be estimated south of 60°S and north of 70°N. The best estimation is obtained between 30°S and 50°N. The error is roughly uniform over the upper 1000m and starts to grow below, particularly for salinity. The data coverage of temperature as well as of salinity

has strongly increased from the year 2003 to the end of 2008 (Fig. 1c and d). However, the number of salinity measurements remain smaller than the number of temperature measurements. This is especially visible at greater depths (Fig. 2c) and will have to be taken into account while estimating global hydrographic variability patterns.

As already noticed in the vertical sections, the data coverage is not uniformly distributed in space and differences exist between the different basins (Fig. 2). It is higher along the equator for temperature in the upper layer, because of the TAO/Pirata moorings. It is also better in the western north Pacific and North Indian Ocean where deployments of Argo floats have been more intense. In the Atlantic, we see the slight deficit in Argo profilers due to the Solo problem that should be solved, at least in part, by ongoing post-processing.

In the next sections we analyze various averages of the individual estimates and it is thus necessary to evaluate the error on these combined products. The estimate $\bar{x}$ of the mean value of a variable x is:

$$\bar{x} = \frac{1}{N} \sum_{i=1}^{N} x_i. \tag{4}$$

Each sample x_i is the sum of the true mean ($\mu(x)$), the variability around the mean (x_i') and the error (e_i):

$$x_i = \mu(x) + x_i' + e_i. \tag{5}$$

The error on the estimate of the mean is thus:

$$E[(\bar{x} - \mu(x))^2] = \frac{1}{N^*}(\sigma_{x'}^2 + \sigma_e^2), \tag{6}$$

where $\sigma_{x'}^2$ is the variance of the samples around the mean, σ_e^2 the variance of the error on each sample and N^* the number of independent samples.

In the case of a time averaging, each monthly analysis is considered as an independent estimate of the anomaly relative to the reference climatology. Thus to compute the error on the mean field over the period 2003-2008 we set $N^* = N = 72$. The corresponding error map is shown Figure 3a and b. To evaluate the error on each annual mean fields we set $N^* = N = 12$.

In the case of space averages, the number of independent data depends on the covariance scales. Since we use gaussian structure functions to define the covariances, the number of 'dependent variables' around a given point is given by the integral over space of the gaussian:

$$\int_0^\infty exp(-q^2x^2)dx = \frac{\sqrt{\pi}}{2q}. \tag{7}$$

Using the largest correlation scales (300 km) gives, $q = 1/(6\sqrt{2})$, and the one side integral equals $6\sqrt{\pi/2}$. Thus for a one dimensional average the number of independent grid points N^* accounts:

$$N^* = \frac{N}{2 * 6\sqrt{\pi/2}} \simeq \frac{N}{15} \quad , \tag{8}$$

where N is the total number of grid points of one dimension (e.g. 720 for a zonal average with a 0.5° grid). For a global average N^* can be evaluated as:

$$N^* = \frac{N}{\pi * 36\pi/2} \simeq \frac{N}{177}. \tag{9}$$

in this case N is the total number of grid points of the global field. As will be seen later in the paper, these errors are significantly smaller than the observed large scale seasonal, interannual and 6-year mean anomaly signals (see Fig. 3). Generally, the signal to noise ratio is high in the upper layer of the tropical basins and at mid-latitudes, i.e. where seasonal to interannual ocean variability appears to be large. This shows that our gridded

fields can be used to analyze such large scale signals. Note that *Roemmich et al.* [2008] also demonstrated the effectiveness of Argo in resolving large-scale ocean variability by using satellite altimetric height as a proxy for steric height.

3. Mean field and annual cycle

In this section we discuss the global fields of ocean temperature and salinity of the upper 2000m depth for the period 2003-2008. We focus on the signatures of hydrographic variability over the water column, first due to long-term changes and second due to the annual cycle. The long-term change is represented by the ARIVO mean (2003-2008) anomaly relative to WOA05. The seasonal cycle is obtained as the 12 month harmonic of the Fourier decomposition of the six year time series. The results are presented as global zonal means.

3.1. The mean 2003-2008 anomaly

The zonal mean temperature of the ARIVO 2003-2008 anomaly at 10m is shown as a function of latitude in Fig. 4a (blue line). A clear hemispheric asymmetry of the difference field can be observed. The anomalies are positive north of 45°S and exceed 0.2°C between 20°N and nearly 70°N. The anomalies drop abruptly south of 45°S and tend to zero. The results of the mean ARIVO near surface estimation can be compared to the satellite derived SST measurements (NSST, http://www.cdc.noaa.gov, NOAA optimum Interpolation SST V2). A similar satellite derived anomaly is built by comparing two time periods, i.e. a short term field during the same period 2003-2008 (NSST_S) and a long-term estimation during the years 1990-2008 (NSST_L). The NSST anomaly is shown as a red line in Fig. 4a. The meridional distribution of the mean anomalies of the ARIVO

2003-2008 anomaly and the NSST difference estimation are similar. In particular, both estimations show low amplitudes in the Southern Ocean, thus ruling out that low values in this part of the global ocean are due to insufficient sampling.

The 2003-2008 mean temperature anomaly at depth is positive at most latitudes and amplitudes are large in the upper 1000m depth, especially in the northern hemisphere (Fig. 4b). Warming patterns are largest in the North Atlantic Ocean, reaching nearly 2000m depth (Fig. 5). Our results are in agreement with the postive temperature trends observed in the studies of LE05 and *Ishii et al.* [2006]. The Southern Ocean is characterized by a weak positive anomaly extending to 1100m depth centered at 40°S that occurs in all three ocean basins which is consistent with the findings of *Gille* [2002], *Cabanes et al.* [2001], *Willis et al.* [2004] and *Ishii et al.* [2006]. In addition, weak warming near Antarctica can be observed in the ARIVO mean anomaly as already noticed by *Willis et al.* [2004].

Regional cooling patterns occur in the tropical subsurface layer and at intermediate depth in the subtropics and tropics, as well as at northern mid-latitudes (Fig. 4b). The cooling at intermediate depth exists in both hemispheres in our results. Its signatures are strongest in the Pacific Ocean, but also appear in the Atlantic on both hemispheres and in the southern tropical Indian Ocean. In the results of LE05 and *Ishii et al.* [2006] the cooling at intermediate depth in the global tropics and subtropics is only observed in the southern hemisphere due to changes in the Pacific Ocean. Other regional cooling is centered at 40°N in deeper layers (Fig. 4b). It is considerably weaker compared to previous estimations [LE05, *Willis et al.*, 2004; *Ishii et al.*, 2006]. These differences suggests that fluctuations in this area persit on interannual and decadal periods which coincides with the explanation of LE05. A similar explanation can be figured out for the pattern at

about 60°N. Our results show warming in the upper 500m depth and a subsurface cooling pattern in this area. A cooling occurs in the results of LE05 and *Ishii et al.* [2006], while warming can be observed in the 10-year temperature trends provided by *Willis et al.* [2004].

The zonal mean salinity ARIVO 2003-2008 anomaly at 10m is shown as a function of latitude in Fig. 4c. Largest differences emerge in the northern tropical ocean in the area of the atmospheric convergence zones associated with freshening in this area [see also *Delcroix et al.*, 2007]. North and south of this peak, 2003-2008 mean salinity anomalies are positive showing patterns of salinity increase in the surface layer of the southern and northern tropics as already noted by *Curry et al.* [2003] and *Boyer et al.* [2005]. North of 30°N the anomalies are positive except at about 40°N. Between 40°-60°S a clear signature of surface freshening can be observed.

This meridional distribution can also be seen at depth (Fig. 4d). As for the temperature changes, anomalous fluctuations from the WOA05 climatology mean state are strongly baroclinic in the upper 500m depth of the tropical basin. Outside the tropics, salinity signatures reach down to 1000m depth and even deeper at higher latitudes. The increase of salinity in the southern subtropics and tropics reach down to about 500m depth. This signature exists in all three ocean basins and is strongest in the Atlantic Ocean. In its northern counterpart, the ARIVO mean salinity anomalies are negative - a pattern which is strongest in the Pacific basin due to a strong La Niña event in 2007, but also exists in the Atlantic and Indian Ocean (Fig. 5, lower panels). Our results differ from previous estimations which showed an increase in salinity of the upper tropics and subtropics in both hemispheres [*Boyer et al.*, 2005; *Ishii et al.*, 2006]. These differences reflect the high

sensitivity of long-term means to strong interannual signatures as ENSO in the tropical basin.

Subtropical and tropical cooling at intermediate depth is accompanied by a freshening in both hemispheres (Fig. 4d) and can be attributed to decreased evaporation-precipitation (E-P) over the polar gyres [*Wong et al.*, 1999]. The signature in the southern hemisphere occurs in all three ocean basins and is strongest in the Pacific, whereas in the northern hemisphere intermediate freshening predominantly emerges in the Pacific Ocean with little evidence in the Atlantic basin (Fig. 5, lower panels). In the analysis of *Boyer et al.* [2005] and *Ishii et al.* [2006] the intermediate freshening is limited to the southern tropics and subtropics.

The difference field of Fig. 4d indicates increasing salinities from about 10°N-77°N in the 0-1000m depth layer. One exceptation occurs in the upper 100m depth centered at about 40°N due to changes in the Pacific basin (Fig. 5). Increasing salinities in the global mean are mostly due to positive anomalies in the North Atlantic and northern Indian Ocean (Fig. 5, lower panels). The results of *Boyer et al.* [2005] and *Ishii et al.* [2006] show a strong and deep reaching freshening signal at 20°N-30°N and 40°N-70°N from the surface down to 3000m depth, mostly in the Pacific Ocean. Our results do not show this pattern in the global zonal mean, but in the Pacific average. Only weak indications of freshening occur in layers below 500m depth. Due to the dominance of the patterns in the previous results and in our results it can be argued that strong decadal fluctuations force the salinity changes in the northern hemisphere - the same result which could be figured out for the temperature estimation.

Deep freshening dominates the Southern Ocean between 40°S-60°S in the upper 1000m of the water column. This deep baroclinic freshening signature occurs in all three ocean basins. Only week evidence of this feature exists in the results of *Boyer et al.* [2005] in the South Pacific and Atlantic as well as in the global mean in this latitude band. Large-scale deep freshening is also reported in the Pacific and Indian Ocean [*Wong et al.*, 1999; *Antonov et al.*, 2002; *Böning et al.*, 2008] which is linked to changes in the atmospheric circulation [*Morrow et al.*, 2008].

3.2. The annual cycle

While the seasonal temperature and salinity changes in the surface layer are well described in the literature [e.g. *Antonov et al.*, 2004; *Boyer and Levitus*, 2002] the global ocean annual cycle at depth is poorly analyzed. Therefore, we focus on the description of the vertical penetration of the annual cycle of the hydrographic field during 2003-2008. The vertical distribution of the seasonal cycle of temperature is illustrated in Fig. 6a for the upper 400m depth. Amplitudes of the annual harmonic of temperature are maximum in the surface layer at mid-latitudes and are characterized by a hemispheric asymmetry with largest amplitudes in the northern hemisphere, reflecting the contrast between the two hemispheres in the distribution of land mass [*Fu and Cazenave*, 2001; *Antonov et al.*, 2004; *Stammer*, 1997]. At mid-latitudes, amplitudes decrease with increasing depth but still exceed 1°C at depth greater than 100m and the explained variance of the annual harmonic accounts for 80% of total variance. In the subpolar regions, surface intensified maxima of the seasonal amplitude of temperature are also observed. One is centered at about 60°S and is known to occur also in some coupled ocean-atmosphere simulations [*Gleckler et al.*, 2006]. Although amplitudes remain small in this region, the annual cy-

cle explains 80% of total variance in our results (Fig. 6a). Another peak appears north of 60°N - i.e. in the area of seasonal sea ice coverage - and the seasonal amplitude as well as its explained variance are high until depth of about 300m. The annual cycle of temperature in the tropical basin is subsurface intensified and exceeds 2°C at about 80m depth. Values of explained variance account for 40% of total variance. Two areas of peaking seasonal amplitudes occur in the tropical subsurface layer, i.e. in the northern equatorial band and centered at about 10°N. These subsurface maxima are associated with dynamical processes mainly triggered by seasonal mixed layer depth variations, seasonal changes of the mean zonal currents and equatorial wave dynamics under the effect of wind stress forcing, rather than surface heating [e.g. *Schott and McCreary*, 2001; *Keenlyside and Kleeman*, 2002; *Arhan et al.*, 2006; *Kessler and Gourdeau*, 2006; *Forget and Wunsch*, 2007].

The use of the ARIVO product allows us to analyze the seasonal cycle of global salinity at depth (Fig. 6b). As can be already seen in previous estimations, the annual cycle of SSS is dominant in regions different from those observed for SST [*Antonov et al.*, 2004; *Boyer and Levitus*, 2002]. Indeed, seasonal amplitudes of salinity at depth increase in areas where seasonal changes of temperature are high, but the largest salinity changes occur in areas where seasonal changes of evaporation, precipitation and ice formation are important (Fig. 6a and b). Moreover, seasonal salinity changes are surface intensified at all latitudes indicating that mostly coupled ocean-atmosphere fluxes trigger the largest seasonal signatures of global ocean salinity, rather than dynamical processes. The global average in Fig. 6b also shows that the space scales of the annual cycle of salinity are

smaller and more regional compared to those of temperature [see also *Reverdin et al.*, 2007, for the Atlantic].

Regions of high amplitudes include the tropical basin and subpolar areas, still exceeding 0.1 below 100m depth especially in the latter domain. In the tropical basin, seasonal salinity amplitudes increase just north of the equator - i.e. in the ITCZ realm - and 40% of variability are explained by the annual cycle in the upper 100m depth. A second peak of seasonal salinity persists just south of the equator and its signatures are weaker and shallower compared to its northern counterpart. Poleward of 60°N, the amplitude of seasonal salinity change is large, and the total variability in this area is explained with 40% by the annual cycle from the surface down to about 200m depth. Enhanced amplitudes south of 60°S - which are mostly located in the Weddel and Ross Sea (not shown) - are confined to the upper 50m depth and the explained variance accounts for more than 60% of total variance. In this area, a second maximum of annual salinity amplitude occurs at 100-200m depth with values between 0.1-0.2. It explains 20% of the total variance. However, the largest amplitudes of the annual cycle of salinity can be observed in the northern hemisphere induced by deep winter convection processes and seasonal ice formation.

4. Interannual fluctuations

The mean seasonal cycle is estimated at each grid point from the temperature and salinity fields over the six years of measurements. The mean seasonal cycle is then removed in order to emphasize interannual variability. The characteristic magnitude of the ARIVO anomalies range between ±0.2°C for temperature and ±0.02 for salinity (Fig. 8). Extreme values exceed ±0.5°C/±0.1 in some parts of the global ocean, mostly occurring in the near

surface layer (not shown). Those ranges of magnitude are of comparable size to previous estimates [e.g. *Levitus and Antonov*, 1997; *Antonov et al.*, 2002]. The estimation on the error of these fields has shown that the values of the large scale anomaly fields are significant (Fig. 3c and d).

The first general view indicates that various types of interannual fluctuations occur in several latitudinal bands of the global ocean, i.e. at mid-latitudes between 30°-60°, in the subtropics between 20°-35° latitudes and in the tropics between 20°S to 20°N (Fig. 7a and b). At mid-latitudes, temperature as well as salinity fluctuations are surface intensified and reach down to depth of more than 1000m. At northern mid-latitudes, standard deviations are strong compared to their southern counterpart reflecting a clear hemispheric asymmetry as could be figured out for the long-term and seasonal variability. Deep reaching interannual fluctuations characterize also the subtropical basins with maxima in the surface layer as well as about 500m depth. In the tropical basins dominant anomalies are mostly confined to the upper 500m depth layer (Fig. 7a). Differences between temperature and salinity fluctuation patterns emerge mostly in the upper layer, predominantly in the tropical band. In the subsurface layers temperature and salinity variations are generally correlated [*Forget and Wunsch*, 2007].

4.1. The mid- and high-latitudes

Overall, the amplitudes of the anomaly fields are largest at northern mid-latitudes. Indeed, the basin-scale of the North Atlantic is considerably smaller than that of the North Pacific but its anomaly field is clearly strongest and variability reaches down to 2000m depth (Fig. 9). Comparable lower temperature and salinity amplitudes can be observed in the North Pacific until depth of 1000m (Fig. 8). In this basin, the meridional space scales

are low and the vertical anomaly field is characterized by strong baroclinic stratifications, especially in the salinity field. The deepest vertical extend of large anomalies is centered at 30°N. Previous results have shown that interannual to decadal changes in the upper North Pacific are associated with the atmospheric PDO forcing [*Carton et al.*, 2008]. At about 60°N deep reaching interannual fluctuations occur which are surface intensified and change sign after 2 years.

In the North Atlantic, meridional space scales are larger and span up to 20° latitude in some years (e.g. in 2003, Fig. 9). The variability patterns of temperature and salinity at depth are associated with deep baroclinic stratifications. Large interannual fluctuations dominate the hydrographic field in the North Atlantic, and temperature and salinity anomalies change sign due to the meridional movements of the subtropical and subpolar fronts [*Eden and Willebrand*, 2001]. Superimposed on these interannual fluctuations are long-term changes. A clear warming and increase in salinity from the year 2003 to 2008 can be observed in the area between 30°N-50°N. A rapid increase of temperature and salinity since the 1990s is also observed in 50 years of hydrographic time series in the northeast North Atlantic and Nordic Seas [*Holliday et al.*, 2008]. A recent increase in salinity due to decadal variability in that area was also reported by *Hatun et al.* [2005]. Furthermore, the findings of *Häkkinen and Rhines* [2004] indicate that those changes are associated with fluctuations of the subpolar gyre strength. North of 60°N, temperature and salinity anomalies increase in the upper 800m depth and anomalies change sign after 2 years. Note that a similar pattern could also be observed in the North Pacific.

The higher latitudes in the Southern Ocean are less stratified which means that interannual changes in the atmospheric forcing at the surface can drive energetic, deep reaching

hydrographic variability [*Speer et al.*, 2000]. This is clearly reflected in our results of Fig. 8 to 10 as large scale fluctuation patterns are characterized by a distinct vertical homogenous structure. Concerning the time scales of variability in the Southern Ocean interannual, decadal changes as well as long-term changes can be observed. Our findings in Fig. 4b show that the changes of the 2003-2008 mean temperature anomaly with respect to the long-term WOA05 mean are weak in this area, whereas the yearly anomalies of Fig. 8 to 10 show large amplitudes. These two findings lead to the conclusion that interannual to decadal variability dominates the temperature changes in that part of the Southern Ocean rather than a long-term trend. In contrast to this, long-term changes in salinity can be observed in our estimation (Fig. 4d). In the yearly anomaly fields, 6-year trends predominantly occur in the Pacific and Indian southern oceans (Fig. 8 and Fig. 10) which coincides with the findings of [*Wong et al.*, 1999; *Antonov et al.*, 2002].

The distributions of anomalies in the upper South Atlantic are different from those in the other basins. *Sterl and Hazeleger* [2003] have shown that the coupled ocean-atmosphere variability in the South Atlantic is largely independent of the variability elsewhere, e.g. no relation with the NAO was found and only a weak one with ENSO. The South Atlantic is unique in transporting energy towards the equator, forming an important link to the Meridional Overturning Circulation (MOC). Ocean-atmosphere interactions in this part of the basin may thus have implications on other domains of the Atlantic Ocean. However, due to the slow propagation of disturbances originating in the southern basin the impact on the hydrographic field in the North Atlantic persists only on long time scales which cannot be addressed in this study.

4.2. The subtropical and tropical basin

Except from the Indian Ocean, the current system in this part of the global ocean is linked to shallow subtropical cells (STCs) which act as a mechanism for transferring mass, heat, salt and tracers between the subduction zones of the subtropical gyres and the equatorial thermocline [e.g. *Schott et al.*, 2004]. In the Indian Ocean, a cross-equatorial cell exists which connects the southern subtropical subduction zone with the upwelling areas in the northern Indian Ocean [*Schott et al.*, 2002]. Through their effect on SST those cells have been proposed as the oceanic component of coupled modes of air-sea variability that influence atmospheric climate on multiple time scales. However, the hydrographic anomaly fields in Fig. 8 to 10 are marked with complex interannual changes in the subtropical basin and superimpose long-term changes as observed in the previous section. Upper layer warming and increase in salinity can be only observed in the subtropical southern Indian basin (Fig. 10). The intermediate cooling and freshening predominantly occurs in the South Pacific subtropics and weak indications also arise in its northern counterpart (Fig. 8). The dominance of interannual fluctuations in this part of the global ocean probably explains the difference in our estimation (Fig. 4b and d) to previous findings, especially in the northern hemisphere. However, due to its complex baroclinic structure hydrographic interannual variability in the subtropics need to be addressed in a more detailed analysis elsewhere rather than in a global analysis.

In the tropical basin, interannual variability is dominant and the changes are marked by a complex baroclinic structure. As expected, the dominant pattern of interannual variability exists in the equatorial Pacific due to the ENSO phenomenon. Largest amplitudes of the temperature field can be observed in 2007/2008 during La Niña conditions

which cover the upper 300m depth of the equatorial basin. Interannual fluctuations of the salinity field are also strong in the equatorial band, especially during the La Niña period. Interesting to note is that during 2006 and 2007 positive salinity anomalies persist in the equatorial basin while temperature changes sign due to the transition from El Niño to La Niña conditions. During the same time, temperature amplitudes increase in the tropical Indian Ocean associated under IOD conditions (Fig. 10). Similar patterns occur in 2003, but weaker and with opposite sign. At the same time, large salinity anomalies can be observed in the upper 500m depth of the tropical basin which extends into the subtropical Indian basin. In 2003, positive salinity anomalies exist in the northern tropics, which change sign south of the equator and become positive again south of 30°S. This meridional tripole pattern reoccurs in 2006 but with opposite sign. Interesting to note is that in each case this pattern reappears one year later, but slightly shifted southward. A similar basin-wide signature is not evident in the temperature anomaly field. In the upper 200m depth of the tropical Atlantic, a meridional dipole pattern in temperature and salinity can be observed in the beginning of our time series with opposite sign in the different hemispheres (Fig. 9). This pattern reoccurs in the year 2006, but only in the salinity field.

4.3. Global averages

Global averages of heat content, freshwater content and steric sea level are evaluated from the ARIVO field during 2003-2008. Heat storage changes are calculated as the integral from 0 to 2000m depth of $\rho c_p T'(z)dz$ where T' is the temperature anomaly presented in the previous section. Freshwater content FW is derived from the salinity anomaly fields

S' as the integral from 0 to 2000m depth of

$$FW = -a \int_z \frac{\rho(T,S,p)}{\rho(T,0,p)} \frac{S'}{(S_r + S')} dz \quad , \tag{10}$$

where a is the area of the global ocean, ρ is the density of seawater, S_r the mean salinity derived from the ARIVO product ($S_r = 34.63$pss) and p is the pressure. Details of this method can be found at *Boyer et al.* [2007]. Steric sea level is calculated as the integral from 10 to 1500m depth of

$$\Delta D = \int_p \alpha(S,T,p) dp - \int_p \alpha(35,0,p) dp \quad , \tag{11}$$

where α is the specific volume which is equal to the inverse of density [*Gilson et al.*, 1998]. The mean seasonal cycle is subtracted from the global average. Error bars of these quantities are evaluated as described in section 2.

Figure 11a shows the variability of globally averaged deep ocean heat content computed from the monthly temperature anomaly fields. A considerable warming is visible from the year 2003 to 2008. The 6-year heat increase implies an average warming rate of $0.77 \pm 0.11 \mathrm{Wm}^{-2}$. Much of this increase in heat storage comes from the Atlantic [Fig. 5, *Levitus et al.*, 2005]. Using satellite altimeter height combined with in situ temperature profiles the analysis of *Willis et al.* [2004] revealed an oceanic warming rate of 0.86 ± 0.12 Wm^{-2} from mid-1993 through mid-2003 in the upper 750m depth. Their warming rate is higher compared to our estimation indicating that either changes in the 750-2000m depth layer or interannual and decadal changes contribute to the average warming. *Levitus et al.* [2005] have shown that the world ocean heat content (0-3000m) increased at a rate of 0.2 Wm^{-2}. This value is much lower since it is an estimation over a much longer time period and earlier.

With the ARIVO product a global average of the freshwater change in the upper 2000m depth can be established for the first years of Argo. Freshwater corresponds to changes in mean salinity that can be due to E-P, river runoff and ice melting. Mass changes due to the import of freshwater from continents are not included. The global average of freshwater content anomalies is dominated by interannual changes. The 6-year trend from 2003 to 2008 is very small (Fig. 11b). During 2003, positive freshwater content can be observed which changes sign in 2004 and 2005. In the years 2006 and 2007, an increase in freshwater content reoccurs.

Globally averaged steric sea level shows a positive trend and the rate of changes from the years 2003 to 2008 can be estimated as 1.01±0.13 mm/year (Fig. 11c). Interannual fluctuations of global steric sea level exist but are small compared to the long term variability. In Fig. 11c, the global mean sea level as measured by satellite altimeter (http: //www.aviso.oceanobs.com/en/news/ocean-indicators/mean-sea-level/index.html) is added for the same time domain (dashed line). On this short time scales based in this analysis, total sea level includes changes due to temperature and salinity related steric expansion as well as mass changes. The total sea level rise based on satellite measurements accounts for 2.34±0.24 mm/year during 2003-2008. Thus, the 6-year changes based on the steric contribution alone constitute about 40% to the total sea level rise during that time. The two time series in Fig. 11c are in good agreement from 2005 through 2007, but diverge from 2003 through 2004 and in the year 2008. Regional biases between the steric and the total sea level can be observed between 30°S to 20°N in those years (Fig. 12). Indeed, the data coverage of the in-situ measurements is lower in the beginning of

our time series (Fig. 1c and d) which probably induces the differences. But this is not the case in the year 2008.

5. Conclusion

Monthly gridded fields of temperature and salinity from the surface down to 2000m depth during 2003-2008 have been used to produce estimates of global ocean hydrographic variability at seasonal, interannual and longer periods. During the six years of in-situ measurements, an oceanic warming of $0.77 \pm 0.11 \mathrm{Wm}^{-2}$ occurred in the upper 2000m depth of the water column. This number is roughly consistent with the 10-year heat content time series published by *Willis et al.* [2004]. Although this represents a significant increase in the rate of warming, the updated long-term study of *Levitus et al.* [2009] shows that the upper ocean (0-700m) heat content increases to a plateau during 2004-2007, i.e. in the time domain of our study. Moreover, our results show large interannual and decadal fluctuations in several areas of the global ocean.

Major advances in measuring the global ocean hydrographic changes have been made by the implementation of the Argo observing system and we have estimated global freshwater content changes. Over the six years of measurements, no significant freshwater rate can be observed as the global average is dominated by interannual fluctuations. But our findings also indicate that large areas of the deep global ocean indeed show long-term tendencies, i.e. in the Southern Ocean. Consistent with our findings, previous studies have examined regional long-term changes in the Southern Ocean which extend deep into the water column [*Roemmich et al.*, 2007; *Morrow et al.*, 2008; *Böning et al.*, 2008].

The rate of global sea level rise and its causes remains a matter of intense debate [*Munk*, 2003; *Cazenave et al.*, 2009; *Willis et al.*, 2008]. We have estimated a steric sea

level rise of 1.01±0.13 mm/year for the 10-1500m depth layer during 2003-2008. This number lies in the range of the estimations during the last decade, but discrepancies are considerably high due to different estimation periods as interannual and decadal changes play a dominant role [e.g. *Stephens et al.*, 2001; *Roemmich et al.*, 2007]. Our results have shown that the sea level from altimetry and steric sea level are in good agreement during the period 2005-2007, but diverge from 2003 through 2004 and in the year 2008. Thus, the 6-year trend deduced from in-situ measurements is lower compared to the satellite derived quantities and 40% of the total sea level rate are due to steric changes. Regional biases between the steric and the total sea level occur in the tropical basin in the years where the two curves diverge. Mass changes as measured by altimetry - which are not included within our steric estimation - probably parts of the differences [see also *Cazenave et al.*, 2009]. Furthermore, the steric height deduced from the ARIVO product is limited to 1500m depth. It is not clear whether changes of the deep ocean largely contribute to the global mean steric sea level or whether barotropic response seen with satellite altimetry lead to the observed differences. Finally, it cannot be excluded that systematic errors still remain in one or more of the global observing systems [*Willis et al.*, 2008].

In addition to the rates of global hydrographic changes, the large-scale spatial patterns of temperature and salinity variability have been estimated. With our findings it is possible to classify time scales of variability within different latitude bands, at least over the period of our in-situ field. These show large amounts of interannual and decadal fluctuations at northern mid-latitudes which reach deep into the water column. Largest and deepest changes occur in the North Atlantic and meridional scales are comparably lower in the North Pacific. The subtropical basins experience rapid heat and freshwater changes at

interannual periods, some of which may have been exported equatorwards, especially in the southern hemisphere. At intermediate depth, cooling and freshening occurs in both hemispheres in the 2003-2008 mean anomaly field with respect to WOA05. A similar distribution can be observed in the tropical basin. Although long-term changes appear in the upper tropical basins, the hydrographic anomaly field is dominated by variability at interannual time scales. At southern mid-latitudes, hydrographic changes occur on interannual to longer time scales and signals spread uniformly over the water column.

Finally, regional differences in time and space between the temperature and salinity variability patterns could be examined. Regions of strong seasonal temperature changes differ from those of the salinity field. Largest amplitudes of the annual cycle of temperature emerge at mid-latitudes in both hemispheres, whereas for the salinity field the amplitudes increase in the tropics and in the subpolar global ocean. Large interannual changes dominate the upper 200m depth of the tropical Pacific, Atlantic and Indian Ocean which are not in phase with those observed in the temperature anomaly field and show up a different baroclinic structure. At southern mid-latitudes, decadal temperature changes are dominant, whereas salinity fluctuations occur on longer time scales.

However, our findings have shown that the global in-situ observing system reveals a large resource of information representing the ocean state in the beginning of the 21th century. New insight of current hydrographic changes could be figured out, especially for the salinity field. With the growing data set of Argo, the estimation of large scale variability and long-term changes from this global observing system - from which our study is part of - will deliver an observational reference field to validate the state of global assimilation models.

Acknowledgments. This work was supported by an IFREMER grant and the European project BOSS4-GMES. Data were made available by the Coriolis data center (Argo-GDAC).

References

Antonov, J., S. Levitus, and T. Boyer (2002), Steric sea level variations during 1957-1994: Importance of salinity, *J. Geophys. Res.*, *107*, doi:10.1029/2001JC000964.

Antonov, J., S. Levitus, and T. Boyer (2004), Climatological annual cycle of ocean heat content, *Geophys. Res. Lett.*, *31*, doi:10.1029/2003GL018851.

Antonov, J., S. Levitus, and T. Boyer (2005), Thermosteric sea level rise, 1955-2003, *Geophys. Res. Lett.*, *32*, doi:10.1029/2005GL023112.

Antonov, J., R. Locarnini, T. Boyer, A. Mishonov, and H. Garcia (2006), World Ocean Atlas 2005, Volume 2: Salinity., *S. Levitus, ED., NOAA Atlas NESDIS, U.S. Government Printing Office, Washington, D.C.*, pp. 182–184.

Argo Data Management (2005), Argo quality control manual V2.1., *(http://www.coriolis.eu.org)*, *ar-um-04-01*, 28.

Arhan, M., A. Treguier, B. Bourlés, and S. Michel (2006), Diagnosing the annual cycle of the equatorial undercurrent in the Atlantic ocean from a general circulation model, *J. Phys. Oceanogr.*, *36*, 1502–1522.

Barnett, T., D. Pierce, K. AchutaRao, P. Gleckler, B. Santer, J. Gregory, and W. Washington (2005), Penetration of human-induced warming into the world's oceans, *Science*, *309*, 284–287.

Böning, C., A. Dispert, M. Visbeck, S. Rintoul, and F. Schwarzkopf (2008), The response of the Antarctic Circumpolar Current to recent climate change, *Nature*, doi: 10.1038/ngeo362.

Boyer, T., and S. Levitus (2002), Harmonic analysis of climatological sea surface salinity, *J. Geophys. Res.*, *107*, doi:10.1029/2001JC000829.

Boyer, T., S. Levitus, J. Antonov, R. Locarnini, and H. Garcia (2005), Linear trends in salinity for the World Ocean, 1955-1998, *Geophys. Res. Lett.*, *32*, doi: 10.1029/2004GL021791.

Boyer, T., S. Levitus, J. Antonov, R. Locarnini, A. Mishov, H. Garcia, and S. Josey (2007), Changes in freshwater content in the North Atlantic Ocean 1955-2006, *Geophys. Res. Lett.*, *34*, doi:10.1029/2007GL030126.

Bretherton, F., R. Davis, and C. Fandry (1976), A technique for objective analysis and design of oceanic experiments applied to Mode-73, *Deep-Sea Res.*, *23*, 559–582.

Cabanes, C., A. Cazenave, and C. L. Provost (2001), Sea level rise during the past 40 years determined from satellite and in situ observations, *Science*, *294*, 840–842.

Carton, J., S. Grodsky, and H. Liu (2008), Variability of the oceanic mixed layer, 1960-2004, *J. Clim.*, *21*, 1029–1047.

Cazenave, A., K. Dominh, S. Guinehut, E. Berthier, W. Llovel, G. Ramillien, M. Ablain, and G. Larnicol (2009), Sea level budget over 2003-2008: A reevaluation from GRACE space gravimetry, satellite altimetry and Argo, *Global and Planetary Change*, *65*, 83–88.

Church, J., and N. White (2006), A 20th century acceleration in global sea-level rise, *Geophys. Res. Lett.*, *33*, doi:10.1029/2005GL024826.

Cummins, P., and H. Freeland (2007), Variability of the North Pacific Current and its bifurcation, *Prog. in Oceanogr.*, *75*, 253–265.

Curry, R., B. Dickson, and I. Yashayaev (2003), A change in the freshwater balance of the Atlantic Ocean over the past four decades, *Letters to Nature*, *426*, 826–829.

Delcroix, T., M. McPhaden, A. Dessier, and Y. Gouriou (2005), Time and space scales for sea surface salinity in the tropical oceans, *Deep-Sea Res. I*, *52*, 787–813.

Delcroix, T., S. Cravatte, and J. McPhaden (2007), Decadal variations and trends in tropical Pacific sea surface salinity since 1970, *J. Geophys. Res.*, *112*, doi: 10.1029/2006JC003801.

Douglass, E., D. Roemmich, and D. Stammer (2006), Interannual variability in northeast Pacific circulation, *J. Geophys. Res.*, *111*, doi:10.1029/2005JC003015.

Eden, C., and J. Willebrand (2001), Mechanism of Interannual to Decadal Variability of the North Atlantic Circulation, *J. Clim.*, *14*, 2266–2280.

Forget, G., and C. Wunsch (2007), Estimated Global Hydrographic Variability, *J. Phys. Oceanogr.*, *37*, 1999–2008.

Fu, L.-L., and A. Cazenave (2001), Satellite Altimetry and Earth Sciences, *International Geophysical Series, Academic Press*, *69*.

Gaillard, F., and R. Charraudeau (2008), ISAS-V4.1b: Description of the method and user manual, *Rapport LPO-08-03, IFREMER Ctr. Brest, France*.

Gaillard, F., E. Autret, V. Thierry, P. Galaup, C. Coatanoan, and T. Loubrieu (2009), Quality control of large Argo data sets, *J. Atmos. Ocean. Tech.*, *26*, 337–351.

Gille, S. (2002), Warming of the the southern ocean since 1950s, *Science*, *295*, 1275–1277.

Gilson, J., D. Roemmich, B. Cornuelle, and L.-L. Fu (1998), Relationship of TOPEX/Poseidon altimetric height to steric height and circulation in the North Pacific, *J. Geophys. Res.*, *103*, 27,947–27,965.

Gleckler, P., K. Sperber, and K.AchutaRao (2006), Annual cycle of global heat content: Observed and simulated, *J. Geophys. Res.*, *111*, doi:10.1029/2005JC003223.

Good, S., G. Corlett, J. Remedios, E. Noyes, and D. Llewellyn-Johnes (2007), The global trend in sea surface temperature from 20 years of advanced very high resolution radiometer data, *J. Clim.*, *20*, 1255–1264.

Häkkinen, S., and P. Rhines (2004), Decline of subpolar North Atlantic circulation during the 1990s, *Science*, *304*, 555–559.

Harrison, D., and M. Carson (2007), Is the World Ocean Warming? Upper-Ocean Temperature Trends: 1950-2000, *J. Phys. Oceanogr.*, *37*, 174–187.

Hatun, H., A. Sando, H. Drange, B. Hansen, and H. Valdimarsson (2005), Influence of the Atlantic subpolar gyre on the thermohaline circulation, *Science*, *309*, 1841–1844.

Holliday, N., S. Hughes, S. Bacon, A. Beszcynska-Möller, B. Hansen, A. Lavin, H. Loeng, K. Mork, S. Østerhus, T. Sherwin, and W. Walczowski (2008), Reversal of the 1960s to 1990s freshening trend in the northeast North Atlantic and Nordic Seas, *Geophys. Res. Lett.*, *35*, doi:10.1029/2007GL032675.

Ishii, M., M. Kimoto, K. Sakamoto, and S.-I. Iwasaki (2006), Steric Sea Level Changes Estimated from Historical Ocean Subsurface Temperature and Salinity Analyses, *J. Phys. Oceanogr.*, *62*, 155–170.

Keenlyside, N., and R. Kleeman (2002), On the annual cycle of the zonal currents in the equatorial Pacific, *J. Geophys. Res.*, *107*, doi:10.1029/200JC000711.

Kessler, W. (1998), Interannual variability of the Subsurface High Salinity Tongue South of the Equator at 165°E, *J. Phys. Oceanogr.*, *29*, 2038–2049.

Kessler, W., and L. Gourdeau (2006), The Annual Cycle of Circulation of the Southwest Subtropical Pacific, Analyzed in an Ocean GCM, *J. Phys. Oceanogr.*, *37*, 1610–1627.

Levitus, S., and J. Antonov (1997), Climatological and Interannual Variability of Temperature, Heat Storage, and Rate of Heat Storage in the World Ocean, *NOAA Atlas NESDIS 16, U.S. Govt. Printing Office, Washington, D.C.*

Levitus, S., J. Antonov, and T. Boyer (2005), Warming of the world ocean, 1955-2003, *Geophys. Res. Lett.*, *32*, doi:10.1029/2004GL021892.

Levitus, S., J. Antonov, T. Boyer, R. Locarnini, H. Garcia, and A. Mishonov (2009), Global ocean heat content 1955-2007 in light of recently revealed instrumentation problems, *Geophys. Res. Lett.*, doi:accepted.

Liebelt, P. (1967), An introduction to optimal estimation, *Addison-Wesley*, pp. 267–269.

Locarnini, R., A. Mishonov, J. Antonov, T. Boyer, and H. Garcia (2006), World Ocean Atlas 2005, Volume 1: Temperature, *S. Levitus, ED., NOAA Atlas NESDIS, U.S. Government Printing Office, Washington, D.C.*, pp. 182–184.

Lombard, A., A. Cazenave, P. L. Traon, and M. Ishii (2005), Contribution of thermal expansion to present-day sea level change revisited, *Global Planetary Change*, *47*, 1–16.

Lyman, J., and G. Johnson (2008), Estimating Annual Global Upper Ocean Heat Content Anomalies Despite Irregular In Situ Ocean Sampling, *J. Clim.*, *in press*, doi: 10.1175/2008JCLI2259.1.

Mignot, J., and C. Frankignoul (2003), On the interannual variability of surface salinity in the Atlantic, *Climate Dynamics*, *20*, 555–565.

Morrow, R., G. Valladeau, and J.-B. Sall/'ee (2008), Observed subsurface signature of Southern Ocean sea level rise, *Prog. Oceanogr.*, *77*, 351–366.

Munk, W. (2003), Ocean Freshening, Sea Level Rising, *Science*, *300*, 2041–2043.

Palmer, M., K. Haines, S. Tett, and T. Ansell (2007), Isolating the signal of ocean global warming, *Geophys. Res. Lett.*, *34*, doi:10.1029/2007GL031712.

Reverdin, G., E. Kestenare, C. Frankignoul, and T. Delcroix (2007), Surface salinity in the Atlantic Ocean (30°S-50°N), *Prog. Oceanogr.*, *73*, 311–340.

Roemmich, D., and W. Gould (2003), The Future of Climate Observations in the Global Ocean, *Sea Technology*, *10*, 10–15.

Roemmich, D., J. Gilson, R. Davis, P. Sutton, S. Wijffels, and S. Riser (2007), Decadal spin-up of the South Pacific subtropical gyre, *J. Phys. Oceanogr.*, *37*, 162–173.

Roemmich, D., M. Belboech, P. Belchi, H. Freeland, W. Gould, F. Grant, M. Ignaszewski, B. King, B. Klein, K. Mork, W. Owens, S. Pouliquen, M. Ravichandran, S. Riser, A. Sterl, T. Suga, M.-S. Suk, P. Sutton, V. Thierry, P.-Y. L. Traon, S. Wijffels, and J. Xu (2008), Argo: the challenge of continuing 10 years of progress, *GODAE Final Symposium*, pp. 1–10.

Saji, N., B. Goswami, P. Vinayachandran, and T. Yamagata (1999), A dipole mode in the tropical Indian Ocean, *Nature*, *401*, 360–363.

Sallée, J., R. Morrow, and K. Speer (2008), Southern Ocean fronts and their variability to climate modes, *J. Clim.*, *21*, 3020–3039.

Schott, F., and J. McCreary (2001), The monsoon circulation of the Indian Ocean, *Prog. Oceanogr.*, *51*, 1–123.

Schott, F., M. Dengler, and R. Schoenefeldt (2002), The shallow overturning circulation of the Indian Ocean, *Prog. Oceanogr.*, *53*, 57–103.

Schott, F., J. McCreary, and G. Johnson (2004), Shallow overturning circulations of the tropical-subtropical oceans, *Geophys. Monogr. Ser.*, *147*, 261–304.

Servain, J., I. Wainer, J. McCreary, and A. Dessier (1999), Relationship between the Equatorial and Meridional Modes of Climatic Variability in the Tropical Atlantic, *Geophys. Res. Lett.*, *26*, 485488.

Speer, K., S. Rintoul, and B. Sloyan (2000), The diabatic deacon cell, *J. Phys. Oceanogr.*, *30*, 32,122–3222.

Stammer, D. (1997), Steric and wind-induced changes in TOPEX/POSEIDON large-scale sea surface topography observations, *J. Geophys. Res.*, *102*, 20,987–21,009.

Stephens, C., S. Levitus, J. Antonov, and T. Boyer (2001), The Pacific regime shift, *Geophys. Res. Lett.*, *28*, 3721–3724.

Sterl, A., and W. Hazeleger (2003), Coupled variability and air-sea interaction in the South Atlantic Ocean, *Climate Dynamics*, *21*, 550–571.

Willis, J., D. Roemmich, and B. Cornuelle (2004), Interannual variability in upper ocean heat content, temperature, and thermosteric expansion on global scales, *J. Geophys. Res.*, *109*, doi:10.1029/2003JC002260.

Willis, J., J. Lyman, G. Johnson, and J. Gilson (2007), Correction to 'Recent cooling of the upper ocean', *Geophys. Res. Lett.*, *34*, doi:10.1029/2007GL030323.

Willis, J., D. Chambers, and R. Nerem (2008), Assessing the globally averaged sea level budget on seasonal to interannual time scales, *J. Geophys. Res.*, *113*, doi: 10.1029/2007JC004517.

Wong, A., A. Bindoff, and J. Church (1999), Large-scale freshening of intermediate waters in the Pacific and Indian Oceans, *Nature*, *400*, 440–443.

Wunsch, C. (1997), The vertical partition of oceanic kinetic energy, *J. Phys. Oceanogr.*, *27*, 1770–1794.

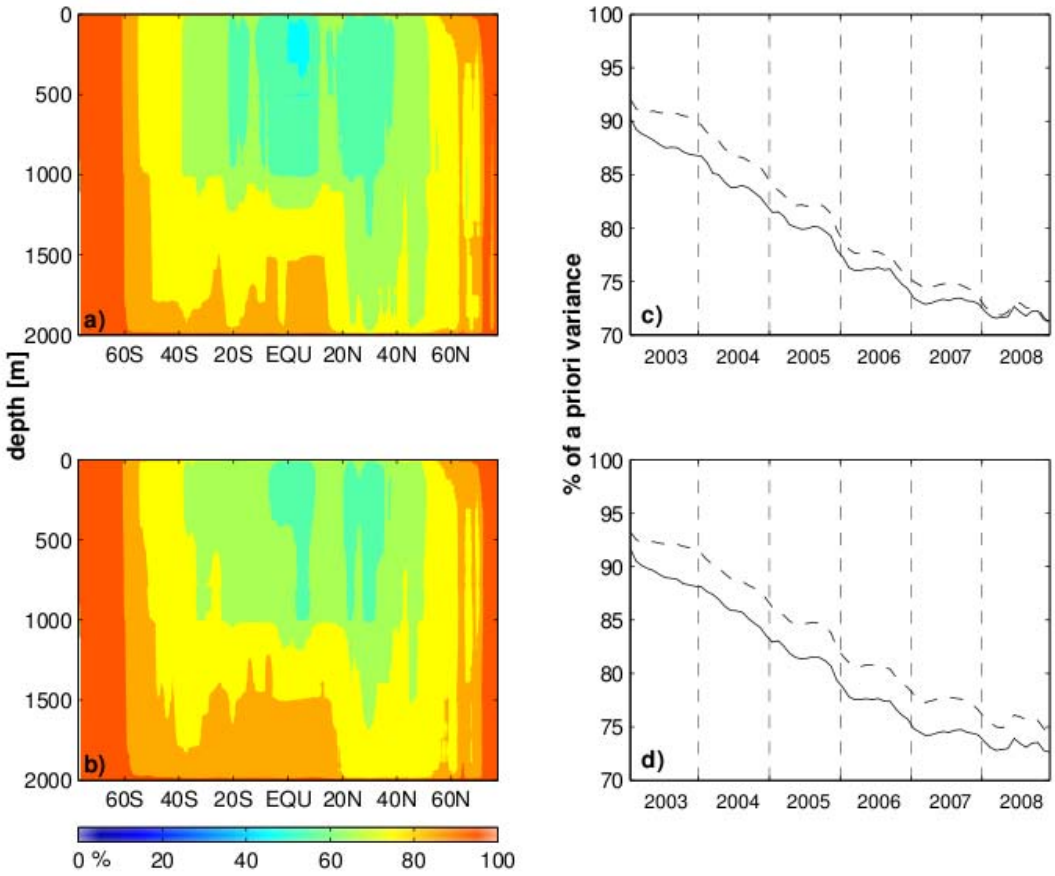

Figure 1. *Global zonal average of percent of a priori variance represented for a) temperature and b) salinity. The statistic parameter is as well averaged in time during 2003-2008. Global zonal integral of a priori variance as a function of time for c) temperature and d) salinity, averaged over the upper 1000m (bold) and over the 1000-2000m depth layer (dashed). A 100% of a priori variance indicates that no information is gained from the measurement field.*

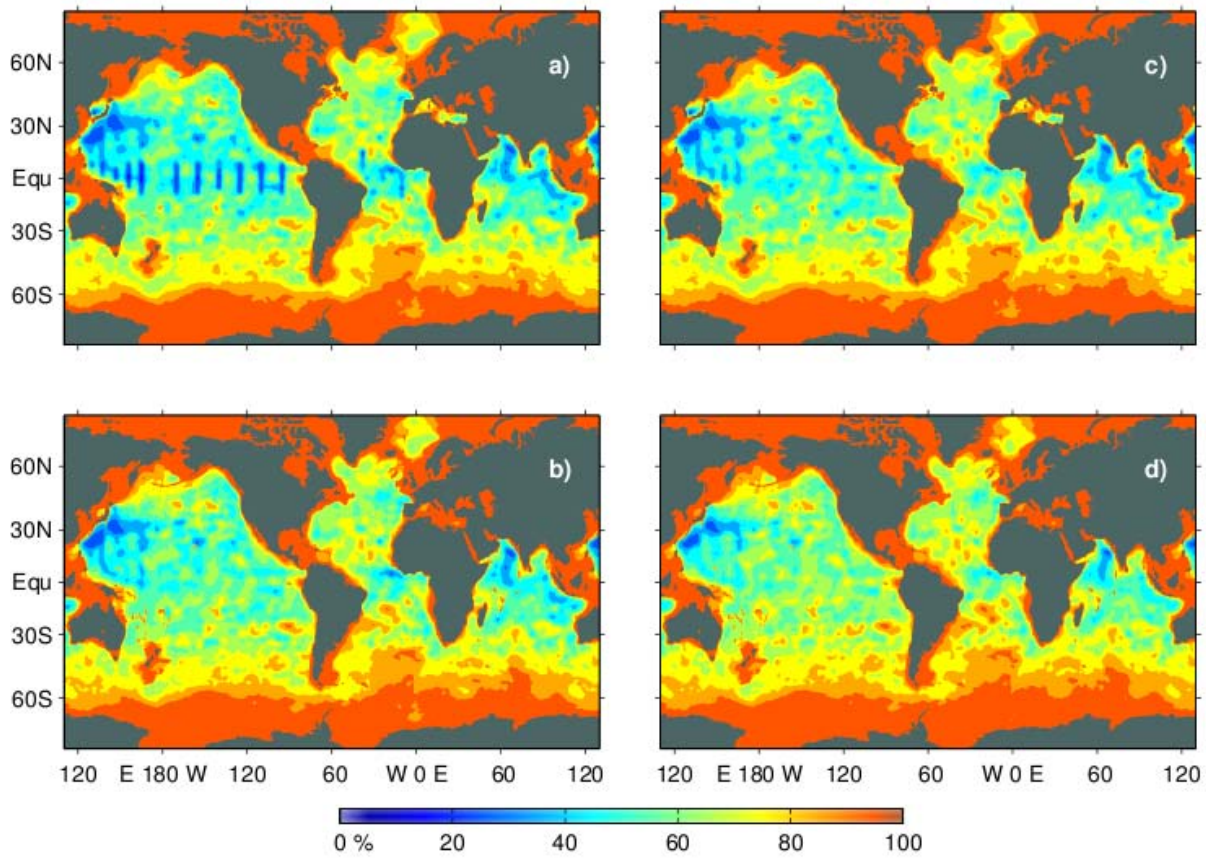

Figure 2. *Horizontal map of percent of a priori variance for temperature (left) and salinity (right) measurements at 100m (a,c) and 1000m (b,d) depth. The statistic parameter is averaged in time during 2003-2008.*

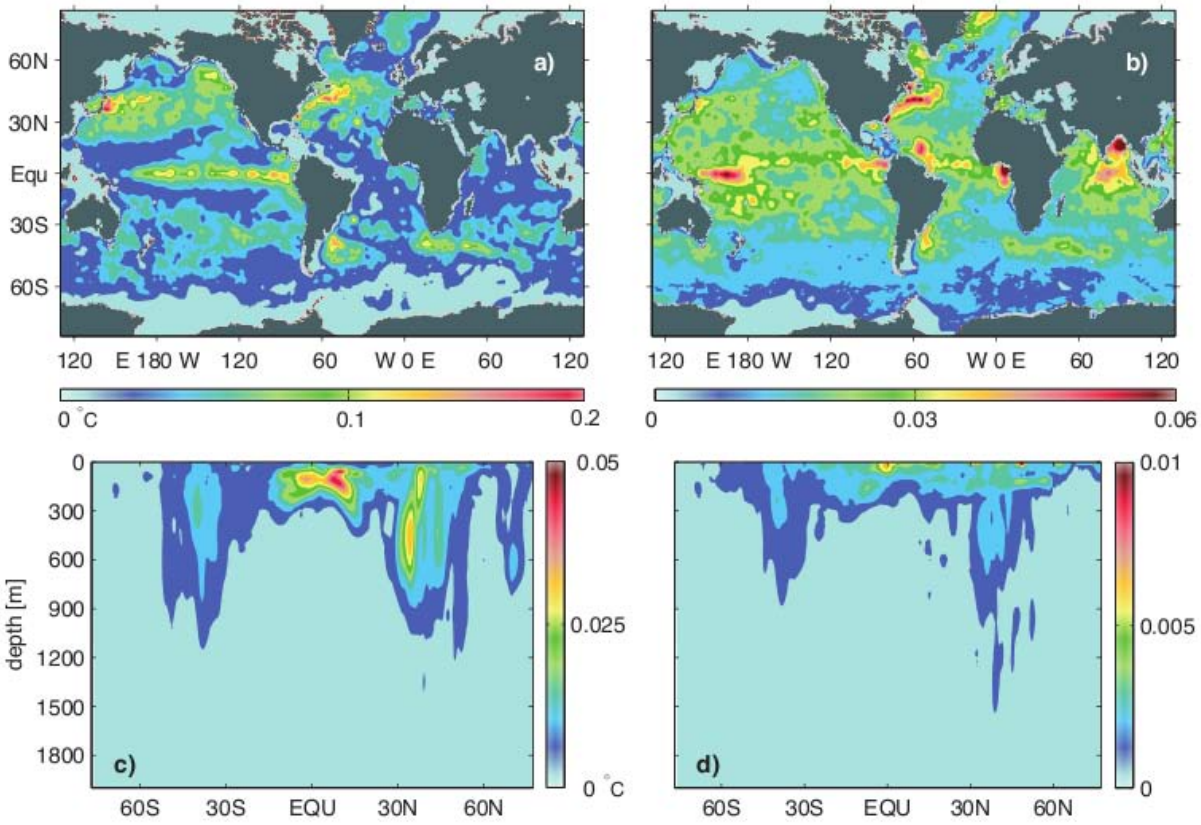

Figure 3. *Error on the mean field over the period 2003-2008 of a) temperature and b) salinity at 10m depth. One dimensional (global zonal) mean of the error on yearly averaged c) temperature and d) salinity as a function of depth.*

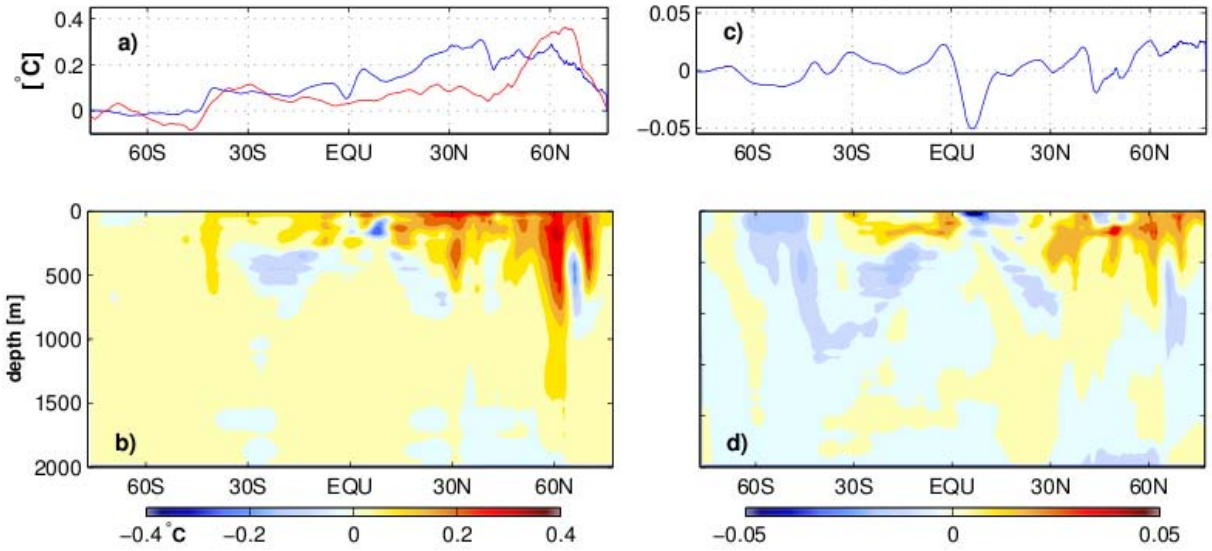

Figure 4. *a) Zonal average of the difference of NOAA optimum Interpolation SST V2 (NSST) of a short-term (2003-2008) minus a long-term (1990-2008, red) mean and of the ARIVO mean anomaly (2003-2008) minus WOA05 temperature at 10m depth (blue), together with the distribution at depth of the latter difference field (b). c) Zonal average of the difference field the ARIVO mean anomaly minus WOA05 salinity at 10m depth and its corresponding vertical distribution (d).*

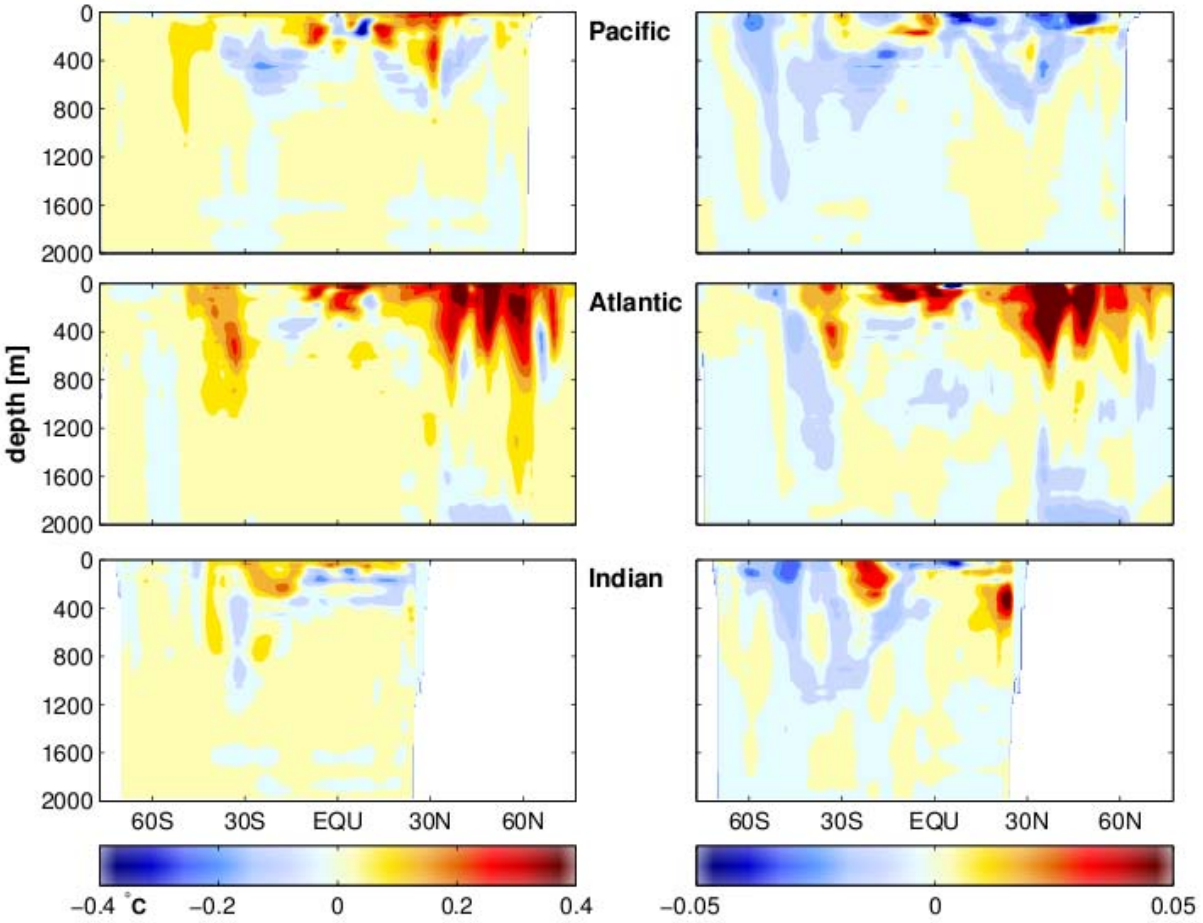

Figure 5. *Basin-wide zonal averages of the difference field mean ARIVO anomaly (2003-2008) minus WOA05 for temperature (upper panels) and salinity (lower panels) at depth.*

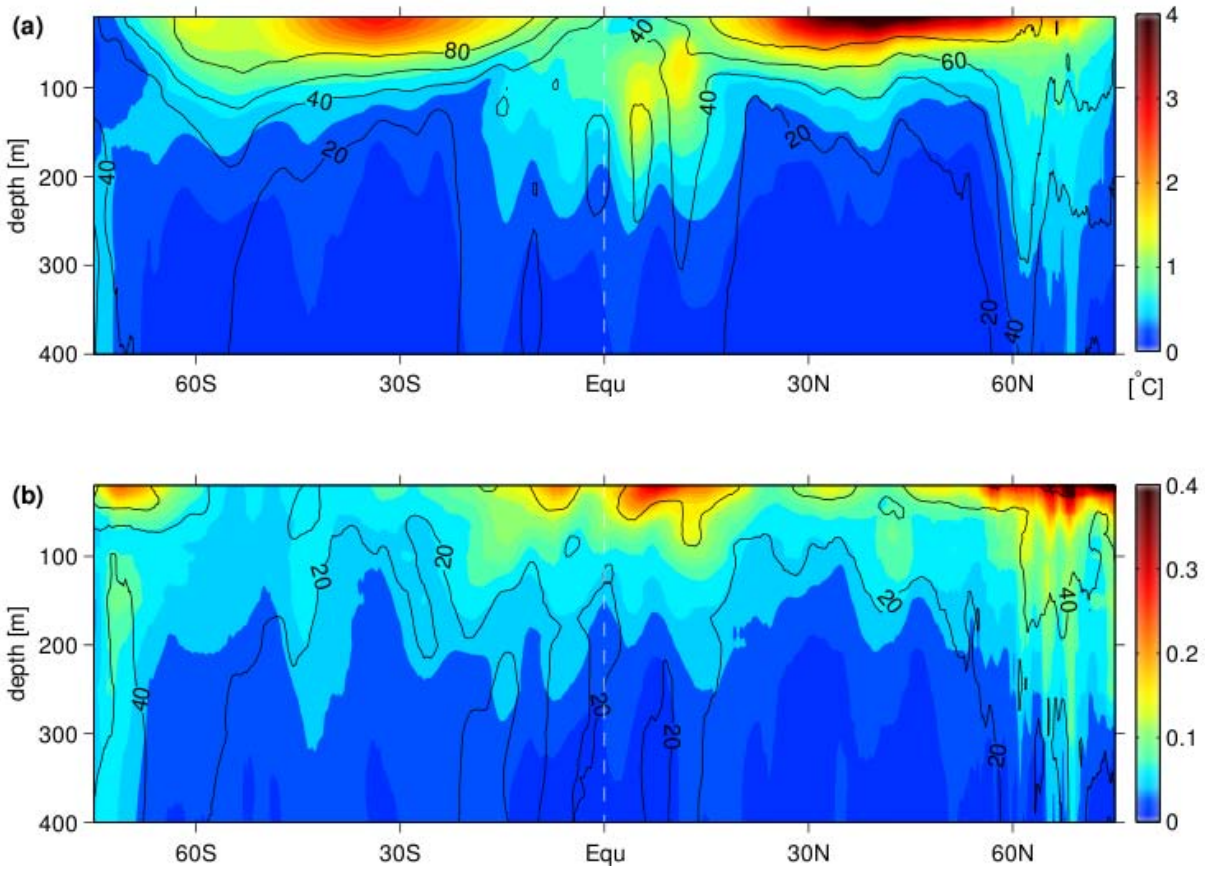

Figure 6. *Global zonal average of the amplitude of the dominant harmonic of ARIVO (a) temperature and (b) salinity in the upper 400m during 2003-2008. Contours show the variance in % explained by the seasonal signal, respectively. White dashed lines indicate the equator.*

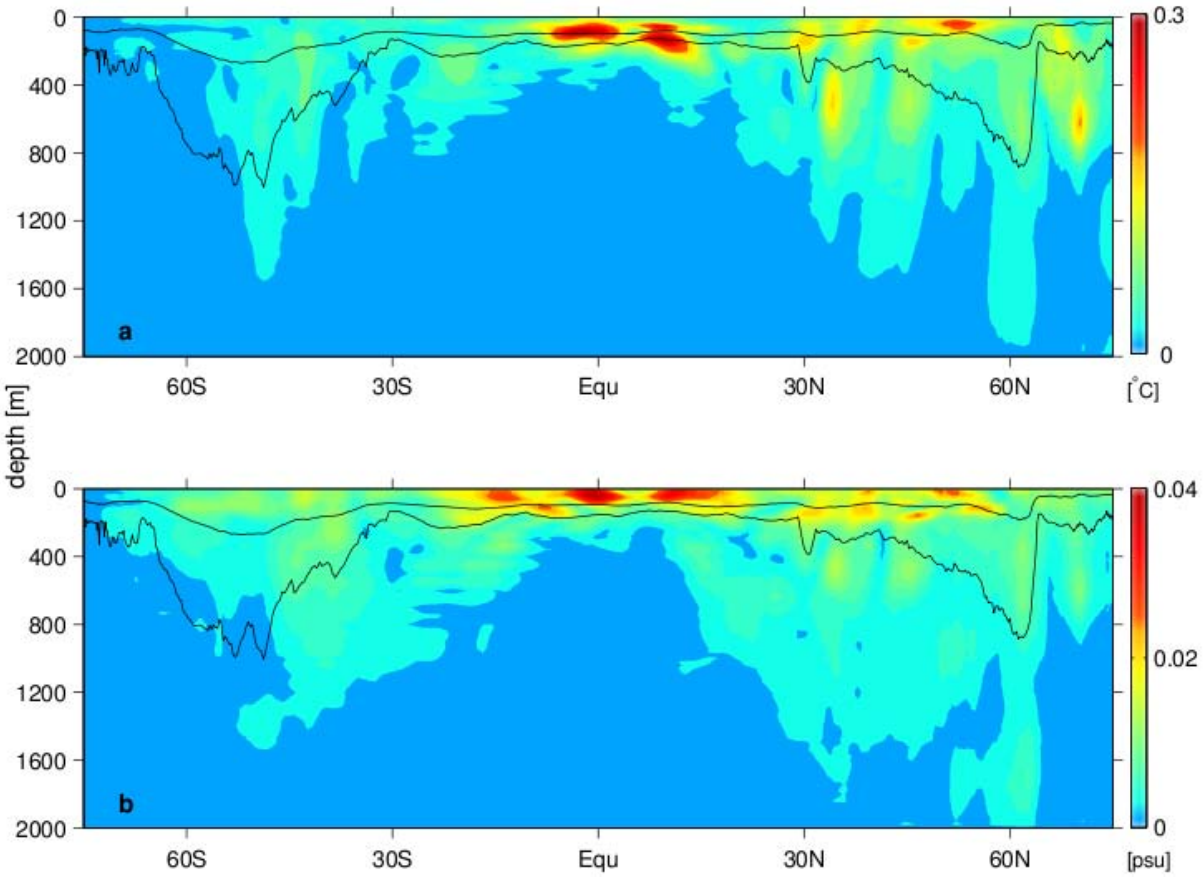

Figure 7. *Global zonal averages of standard deviations of annual mean a) temperature, b) salinity derived from the ARIVO anomaly field 2003-2008 from the near surface layer down to 2000m depth. Mean and maximum pycnocline depths are added (black line).*

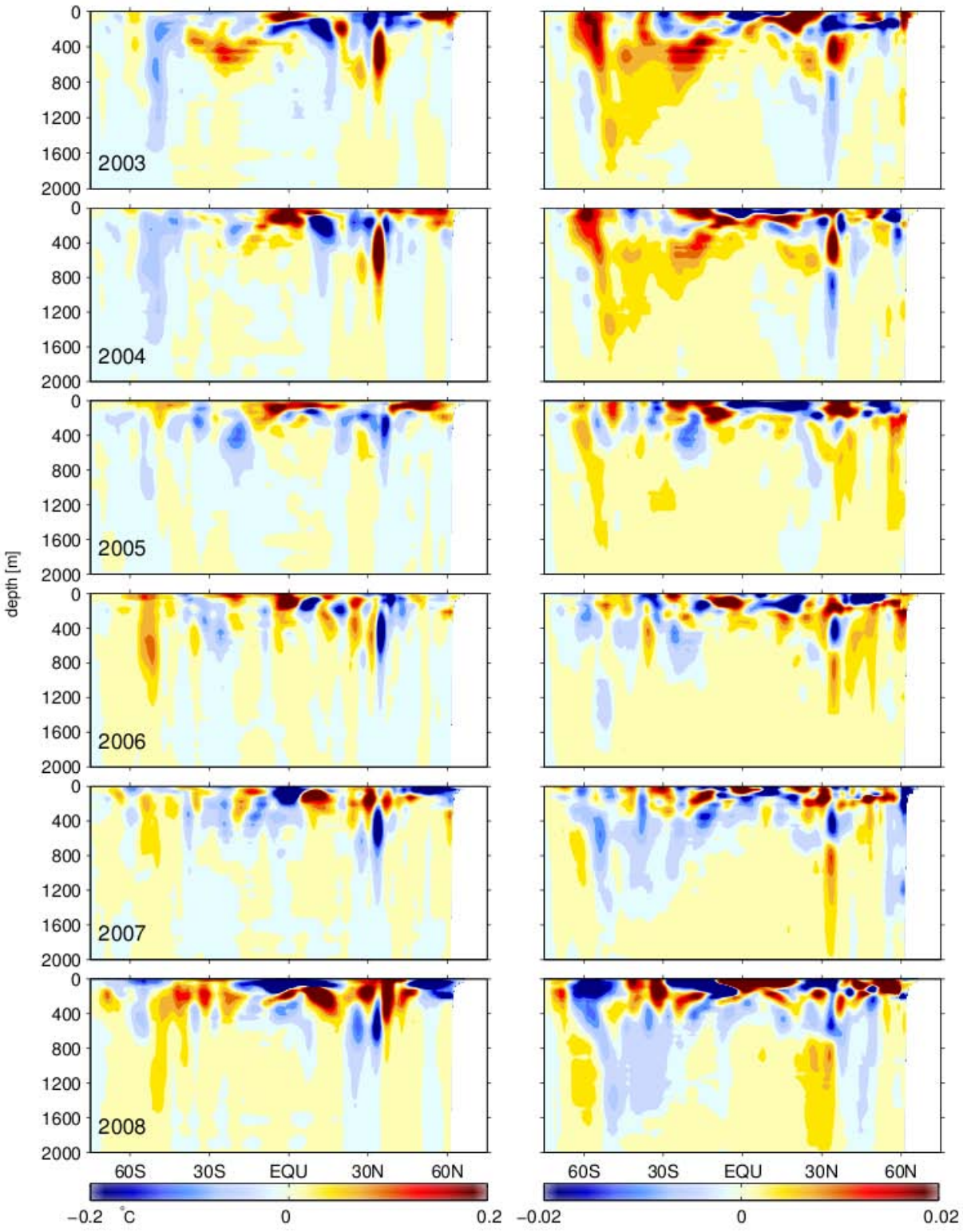

Figure 8. *Yearly zonal average of temperature (left) and salinity (right) anomalies in the Pacific basin during 2003 to 2008 for the upper 2000m depth.*

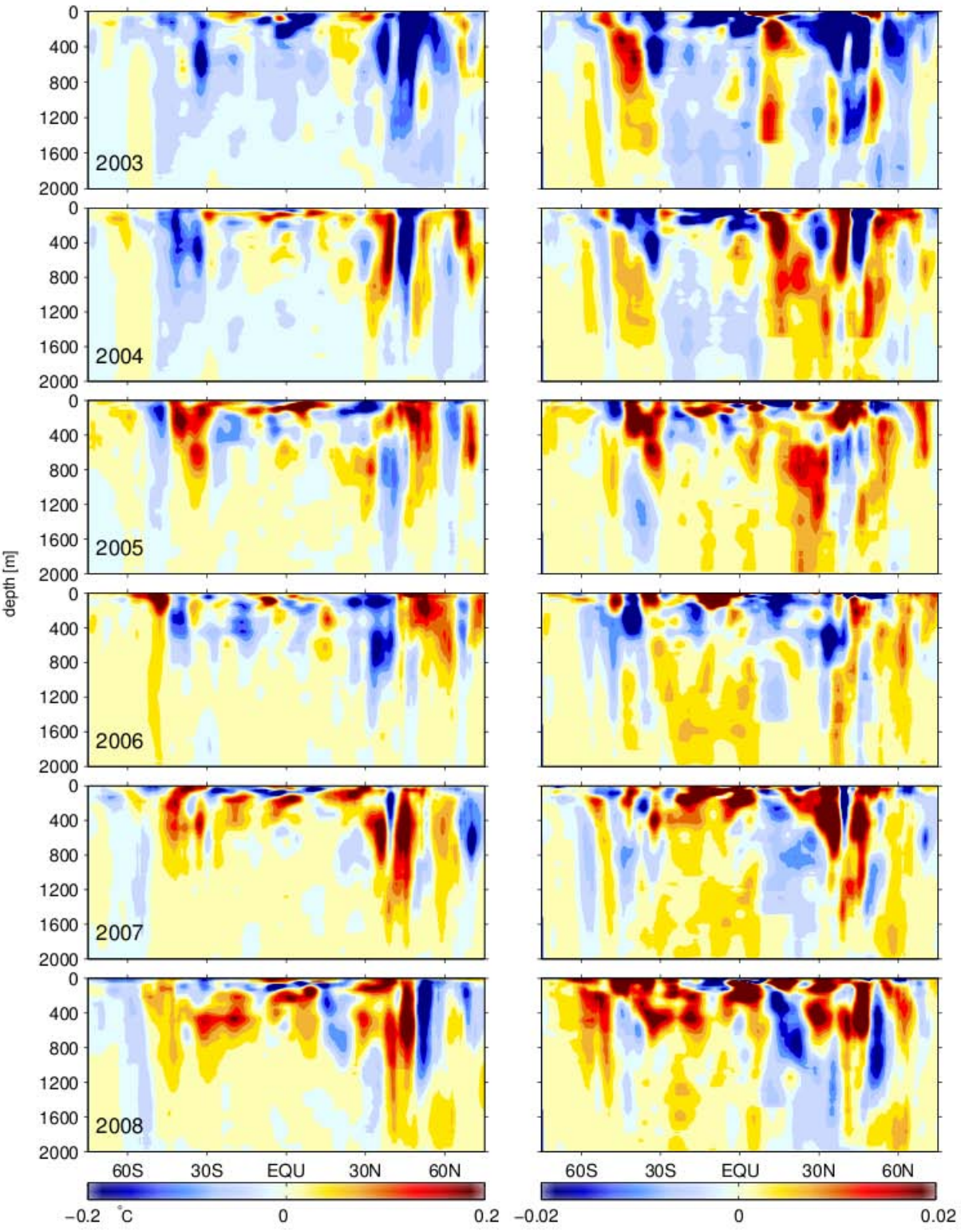

Figure 9. *Same as Fig.8, but in the Atlantic basin.*

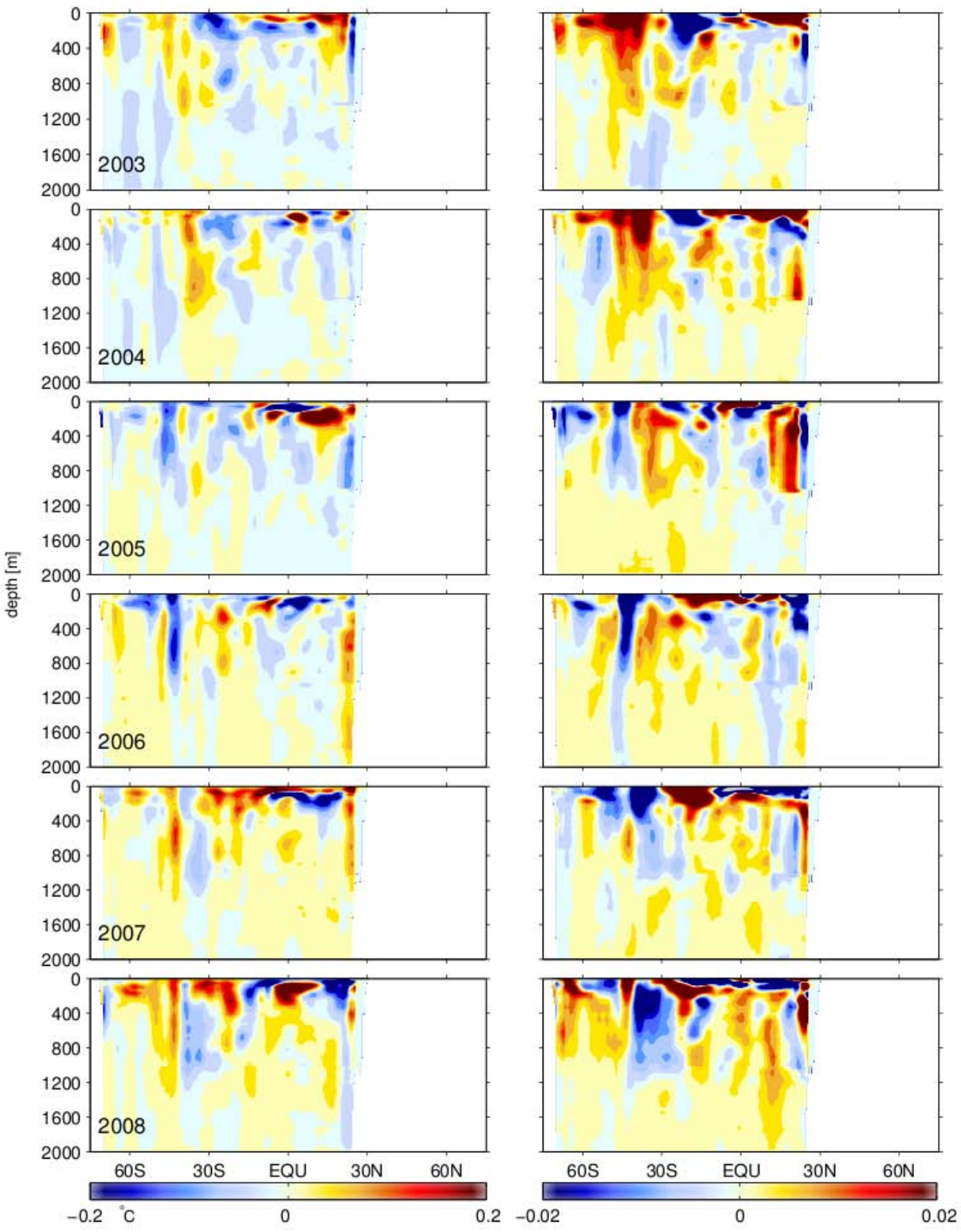

Figure 10. *Same as Fig.8, but in the Indian basin.*

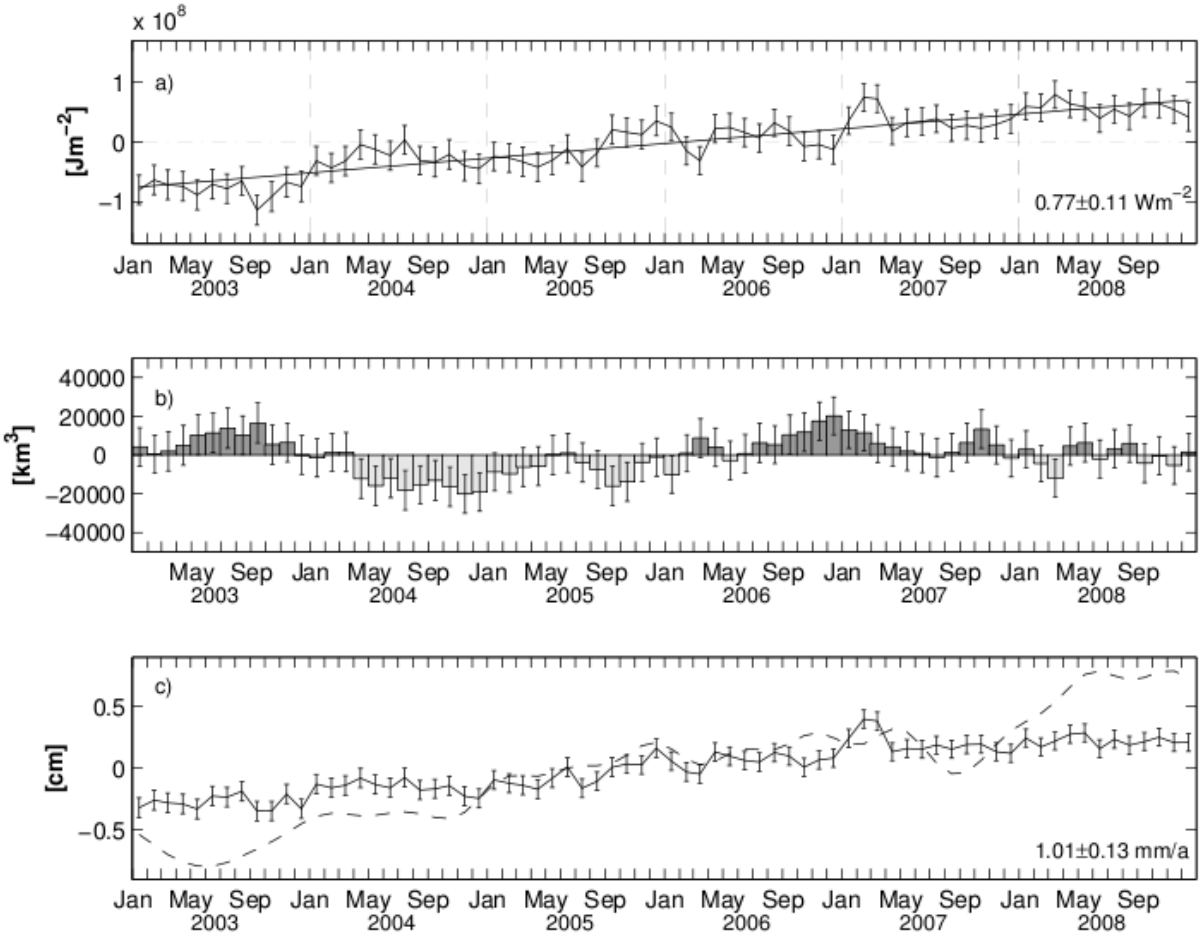

Figure 11. *Time series of global mean a) heat storage (0-2000m) b) freshwater content (0-2000m) and c) steric height (10-1500m). The global mean sea level as measured by satellite altimetry (www.aviso.oceanobs.com/en/news/ocean-indicators/mean-sea-level/index.html) is added in c) with a dashed line.*

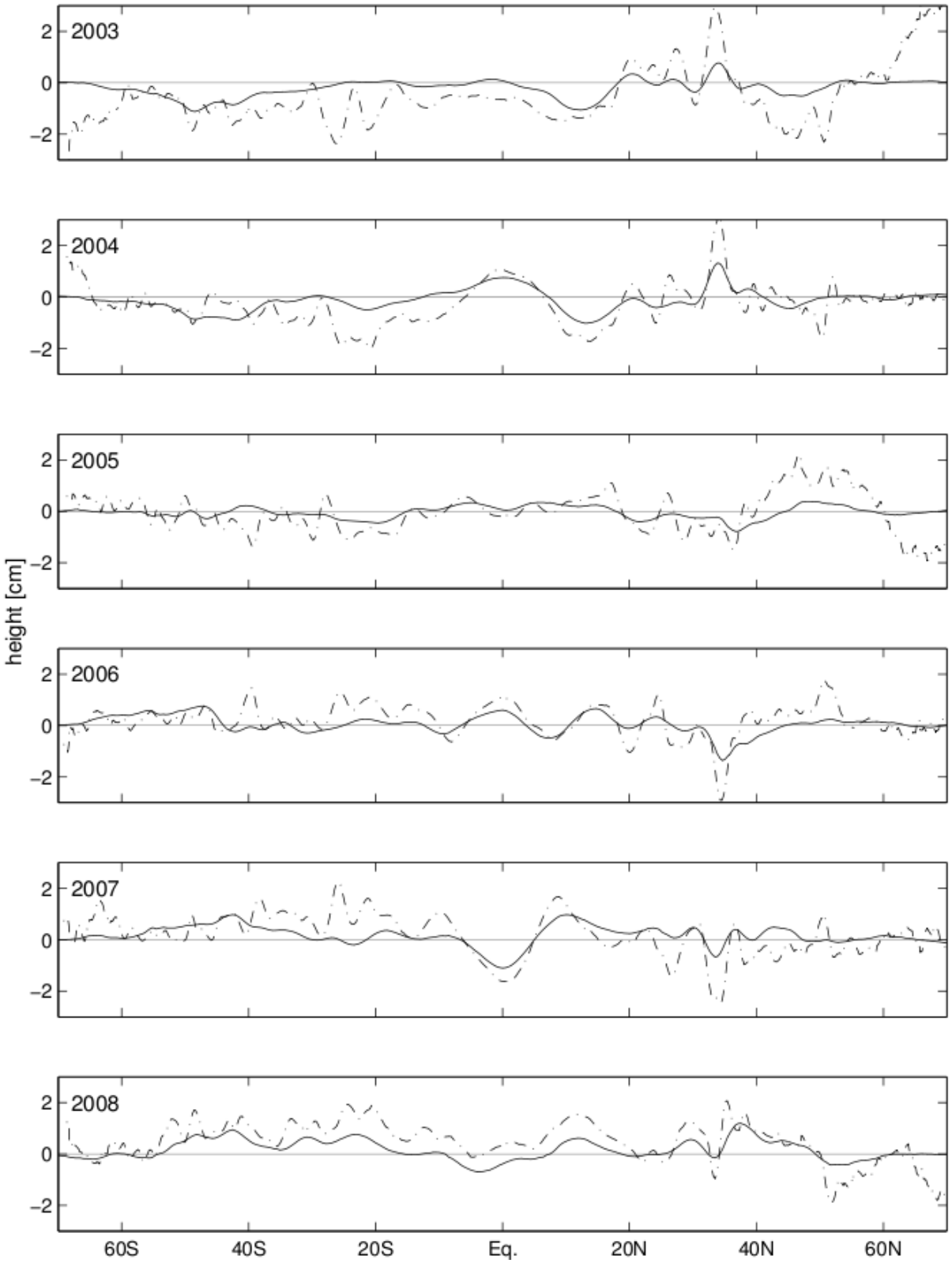

Figure 12. *Yearly global zonal average of steric height (10-1500m, solid) and the corresponding satellite derived sea level anomalies (www.aviso.oceanobs.com, dashed dotted) during 2003-2008 (note that only the first week of December 2008 was available in delayed mode).*